Spectral radiation emitted by kerosene pool fires

Gilles Parent, Giacomo Erez, Anthony Collin, Mathieu Suzanne, Aurélien Thiry-Muller, Mathieu Weber, Eddie Faure, Pascal Boulet

Accepted Manuscript

Spectral radiation emitted by kerosene pool fires

Gilles Parent, Giacomo Erez, Anthony Collin, Mathieu Suzanne, Aurélien Thiry-Muller, Mathieu Weber, Eddie Faure, Pascal Boulet

PII: S0379-7112(19)30042-6

DOI: https://doi.org/10.1016/j.firesaf.2019.102847

Article Number: 102847

Reference: FISJ 102847

To appear in: *Fire Safety Journal*

Received Date: 14 January 2019

Revised Date: 2 July 2019

Accepted Date: 3 July 2019

Please cite this article as: G. Parent, G. Erez, A. Collin, M. Suzanne, Auré. Thiry-Muller, M. Weber, E. Faure, P. Boulet, Spectral radiation emitted by kerosene pool fires, *Fire Safety Journal* (2019), doi: https://doi.org/10.1016/j.firesaf.2019.102847.

Spectral radiation emitted by kerosene pool fires

Gilles Parent[a], Giacomo Erez[a,b], Anthony Collin[a], Mathieu Suzanne[b], Aurélien Thiry-Muller[b], Mathieu Weber[a], Eddie Faure[b], Pascal Boulet[a]

[a] *Laboratoire Énergies et Mécanique, Théorique et Appliquée (LEMTA), Université de Lorraine, CNRS, 2 Avenue de la Forêt de Haye TSA 60604 – 54518 Vandœuvre lès Nancy Cedex, France*
[b] *Laboratoire Central de la Préfecture de Police (LCPP), 39bis Rue de Dantzig, 75015 Paris, France*

Abstract

We present an equivalent medium model that considers emission from the flame volume to compute spectral radiation intensities. This is considered a more detailed description than common radiation models used in fire safety applications, which often treat the flame as a grey emitting surface. Given its importance in fire radiation, the present study focuses on emission by soot. The required parameters for the model are an equivalent absorption coefficient, and an equivalent temperature. They were determined using two independent measurements, namely multispectral opacimetry, and infrared spectrometry. Results are presented for kerosene pool fires (widths from 30 cm to 250 cm). It is shown that the equivalent temperature can be considered independent of flame size, and thus an intrinsic parameter of the fuel. These results also make clear that radiation emitted from the flame is not grey, and can only be considered black for very large flames (i.e. wider than 1.75 m for present tests).

Keywords: radiative heat transfer, pool fire, multi-scale, opacimetry, spectrometry

1. Introduction

Characterising radiative heat flux emitted by a fire is of primary importance because it is the main heat source involved in vaporisation or pyrolysis of the fuel (for flames sufficiently large, i.e. wider than approx. 0.2 m [1]). Mass loss rate (MLR) and consequently heat release rate (HRR) are then driven by radiative heat flux. More generally, radiation is also a major parameter controlling fire spread [2] and propagation to distant combustible targets.

Flames studied in fire science are turbulent diffusion flames, with fast and large spatial variations of species (combustion gases and soot) concentrations and temperature. A comprehensive description of such flames is out of reach experimentally and numerically, and is not necessary because time and space averaged heat fluxes are sufficient to compute the energy received by the fuel. Simplifications are thus made, and in fire science flame radiation is often assumed to be emitted by an equivalent grey surface ("solid flame model") with a flux density equal to

$$\Phi = \epsilon \sigma_{\mathrm{B}} T^4. \tag{1}$$

In this expression two quantities have to be determined, namely the flame temperature T and the flame emissivity ϵ (σ_{B} is the Stefan-Boltzmann constant). The flame temperature can be measured using thermocouples, but attention must be paid to account for heat losses (mainly radiative), otherwise the temperature can be largely underestimated. An example of such correction is given in [3]. Regarding the flame emissivity, several approaches have been developed, as described in a recent and comprehensive review by Raj *et al.* [4]. The experimental methodologies listed in their work can be summarised into four main classes. The first one is based on a simple heat balance at the surface of the combustible proposed by Babrauskas [1]. In this approach, flame emissivity is simply related to the MLR of the pool fire. It is noted that this emissivity is then a mean emissivity of the flame seen from the combustible surface. The second one is based on the radiative heat fluxes measured by fluxmeters around the fire [5–7]. By using radiative view factors the heat flux emitted by the flame can be estimated. In this way a global emissivity for the flame is obtained. The third one relies on flame transmittance measurements. Indeed, the flame emissivity ϵ can be related to its transmittance $\mathcal{T}$ by the relation $\epsilon = 1 - \mathcal{T}$. In these methods, one [8–11] or several [4, 6, 12–15] heaters are put behind the flame, and an infrared camera looks at this/these heater(s) through the flame. In [4] and [15], 40 electrically heated strips were used, allowing to compute temperature and emissivity maps of the flame. The last class of methods is related to two-colours pyrometry [16], multicolour pyrometry, or even to hyperspectral imaging [17]. In these methods, both emissivity and temperature are theoretically obtained at the same time. Regarding two-colours pyrometry, a grey emissivity (same

Email address: gilles.parent@univ-lorraine.fr (Gilles Parent)

emissivity for both wavelengths) is assumed, which is not true for a flame as will be shown in the present paper. Assessing the error due to this approximation is difficult.

Except multicolour pyrometry and hyperspectral imaging, all the techniques mentioned before assume that the flame is grey, or give a grey equivalent flame emissivity. But it is known that, in the general case, radiative flame properties are not grey. This is particularly true for small flame thicknesses (e.g. $< 0.20\,\mathrm{m}$ as cited in [6]), for which radiation comes predominantly from combustion gases that emit in precise wavelength ranges, and not at all in other ranges. For intermediate size flames, soot becomes a significant, or even predominant, contributor to the emission [18]. The spectral dependence of the absorption coefficient $\kappa(\lambda)$ for soot (and then the spectral emission coefficient by virtue of Kirchhoff principle) are generally described by the Rayleigh theory which states that $\kappa(\lambda) = 6\pi E(m) f_\mathrm{v}/\lambda$. In this relation, f_v is the soot volumetric fraction, λ the wavelength, and $E(m)$ a function of the so-called optical parameter m (see Appendix A). As an approximation, $\kappa(\lambda)$ is often described by a simpler expression [19]

$$\kappa(\lambda) = \frac{C f_\mathrm{v}}{\lambda^\alpha}, \tag{2}$$

where α is a coefficient dependent on the fuel type.

When the flame width e increases, its optical thickness $\tau(\lambda) = \kappa(\lambda) e$ increases as well. Ultimately, the flame becomes opaque, and thus emits like a blackbody. According to data available in the literature, the required flame thickness to reach this limit is equal to several meters. For hydrocarbons pool fires, this size is in the order of 3 m [20]. For forest fuels, authors report flame emissivities close to that of a blackbody (i.e. 0.90) for fire widths greater than 2 m to 4.8 m [6].

For combustible materials with (almost) wavelength-independent absorption, a grey description of the radiation emitted by the flame is a satisfactory approach to assess heat transfer from the flame to the combustible. But many fuels, including alcohols [21], hydrocarbons [22, 23] and polymers [24, 25], actually behave as highly non-grey materials with some transparent, semi-transparent and opaque spectral windows. Particularly several of these fuels are perfectly transparent in visible and near-infrared ranges, and opaque in mid-infrared and beyond. This results in differences depending on the radiation source. As an example, it was shown in [25] that absorption by PMMA changes when exposed to a fire propagation apparatus (FPA), which has a high level of radiation in visible and near-infrared ranges, or a cone calorimeter, which emits mainly in mid-infrared. The same applies when considering radiation from fires. Indeed, given the emissive properties of soot (see Equation 2), the emissivity of a flame is expected to be higher at visible and near-infrared wavelengths, where the materials mentioned before are almost transparent. This illustrates the importance of a spectral description of flame radiation to correctly model absorption by this kind of materials.

Spectral characterisations of large flames were reported only in a few papers. Suo-Anttila *et al.* [22] gathered emission spectra of radiation from 2 m diameter pool fires, for several liquid fuels. Spectral range was between 1.3 and 4.8 µm. In their work, emission spectra were recorded through a sight tube allowing to measure "downwards" radiation, from the flame to the combustible. The tube tip height was varied from a few centimetres up to 1 m above the fuel surface. Combustion gases were the primary emitters for ethanol fires, while soot dominated for an ethanol/toluene mixture, JP-8, and heptane. For these three fuels, radiation was attenuated in the lower region of the flame due to absorption by H_2O, CO_2, fuel vapour, and soot. In [26], emission spectra of small wood fires (tray size $50 \times 50\,\mathrm{cm}^2$) showed that emitted radiation was located in precise spectral ranges typical of combustion gases radiation. Soot emission levels were very low for such flame size. In [27], larger wood fires (from 0.5 m up to 4 m wide) were investigated. For the largest fire sizes, a high emission level coming from soot was observed, but the flame was still not black. Assuming an opaque flame ($\epsilon = 1$) for the largest fire size and the smallest wavelengths (for which κ is the greatest according Equation 2), a temperature close to 1400 K was obtained. Still for the largest fire size, the emissivity was found to be only 0.5 at wavelengths near 10 µm, showing the highly non-grey behaviour of flame emissivity. Spectral measurements performed on large scale kerosene pool fires were reported in [28]. The present paper is an extension of this study with more results provided and an extended analysis.

As stated in the introduction, a fully resolved characterisation of fire flames, that is a complete spatial and temporal description of medium to large flames, is nowadays out of reach, and the complexity of such data would anyway be unusable in most practical cases. On the other hand, a grey surface flame model suffers from a number of insufficiencies described hereabove. The objective of the present work is thus to propose a model in which radiation coming from the flame is no longer considered to be emitted from an equivalent surface but instead is emitted from the flame volume itself. To have a model simple enough to be used in fire sciences, a homogenous isothermal medium is used to model the flame. In order to describe this equivalent medium, temperatures and absorption coefficients have to be determined. The present flame volume model will have a particular interest, especially compared to the surface model, if identified properties (equivalent temperature and absorption coefficient) are not, or weakly, dependent on the flame thickness.

This work focuses on soot radiation. Indeed, soot is the major radiation emitter for medium to large scale fires, as emission from gases is located in reduced spectral bands (e.g. the CO_2 band around 4.5 µm) for which the flame becomes opaque even for quite small thicknesses. Moreover, a significant part of this emission by combustion gases is absorbed by cold atmospheric CO_2 and H_2O. Because of the non-grey properties of soot, a spectral approach is ne-

cessary, but can be analytical, as it will be shown.

In a first step, we studied kerosene pool fires, and measurements were performed along a horizontal line of sight, ten to twenty centimetres above the pool. This height was chosen because the thickness of the flame is easier to determine there (width nearly equal to the pool size). Complementary work will have to be done to see if there is a significant sensitivity of the equivalent medium parameters with the position and the orientation of the emitted radiation. Ideally, this model could be accurate enough to allow calculation of radiative heat fluxes received everywhere in space given only the flame geometry.

Experimentally, the radiation coming from the flame was measured by a Fourier transform infrared (FTIR) spectrometer in the spectral range $800\,\mathrm{cm}^{-1}$ to $6000\,\mathrm{cm}^{-1}$ (i.e. $12.5\,\mu\mathrm{m}$ to $1.67\,\mu\mathrm{m}$). This radiation is the result of the emission by combustion gases and soot along the line of sight of the spectrometer. Along this path, concentration of species and temperature inside the flame are highly heterogeneous, and vary quickly due to the highly turbulent nature of the flame. As said above, an equivalent homogeneous and isothermal medium was considered instead of these actual properties. In such a medium, the resolution of the radiative transfer equation (RTE) that describes the evolution of the spectral radiant intensity $I_\lambda(s)$ along the curvilinear coordinate s is analytical [19] (soot scattering being neglected as discussed in Appendix A). At the exit point of a medium of thickness e, the intensity is given by

$$\begin{aligned} I_\lambda(s=e) &= (1-\mathcal{T}(\lambda))I_\lambda^{\mathrm{bb}}(T) \\ &= (1-\exp\left(-\kappa(\lambda)e\right))\,I_\lambda^{\mathrm{bb}}(T), \end{aligned} \tag{3}$$

where $I_\lambda^{\mathrm{bb}}(T)$ stands for the blackbody intensity at a temperature T [19], and $\mathcal{T}(\lambda)$ for the flame transmittance. The latter is related to the flame width e and absorption coefficient $\kappa(\lambda)$ by the Beer-Lambert law: $\mathcal{T}(\lambda) = \exp\left(-\kappa(\lambda)e\right)$. At this stage, the radiation intensity is still dependent on two quantities: the equivalent flame temperature T and the flame transmittance $\mathcal{T}(\lambda)$. This is similar to the usual surface flame model in Equation 1, where temperature and flame emissivity were needed. Two independent measurements should thus be performed. In this work, emission spectra were gathered along with transmittance values, determined by using several laser beams crossing the flame. Laser wavelengths were chosen outside gases absorption bands, so only soot absorption, and consequently emission, was studied.

2. Experimental setup

2.1. Overview

Two test sites were used to conduct the experiments, depending on the fire size. The first was a former aircraft hangar (approx. $300 \times 50 \times 17\,\mathrm{m}^3$, length × width × height, see Figure 1), gracefully lent by Groupe ADP (Orly, France). It easily accommodated the largest fires so they could be considered well ventilated while being shielded from wind and rain. The second was the PROMETHEI experimental facility (LEMTA, Nancy, France). This smaller hangar (approx. $20 \times 15 \times 7\,\mathrm{m}^3$) was used for the tests with pool size less than $1\,\mathrm{m}^2$. The setup was similar for both sites (the main differences are due to the higher heat fluxes experienced during the large fires), and is described hereafter.

Figure 1: View of a $6\,\mathrm{m}^2$ kerosene pool fire in Orly. The opacimetry setup (behind brick walls) can be seen to the left and right of the fire.

The fuel used for the present work was Jet A-1 (NATO code F-35) kerosene. Pool fires were performed in square steel pans. The ones used in Orly (widths of 250 cm, 175 cm, 100 cm and 70 cm) had a height of 20 cm and a thickness of 4 mm, and the ones used in Nancy (widths of 70 cm, 50 cm and 30 cm) a height of 5 cm and a thickness of 2 mm. The lip size (height of pan edge above the fuel surface) was approximately 5 cm at the beginning of the large tests, and 4.5 cm for the small ones. The fuel height was not kept constant, and the tests were conducted until flame out. For the largest fires performed in Orly, the fuel was laid on water to regulate combustion, and the tests were started by igniting a small layer of ethanol poured beforehand on top of the kerosene. This additional fuel was burned during the first minute of the fire, and thus considered to have a negligible influence on the results.

Most of the tests were performed using load cells to monitor mass loss. Only the largest pool fire (approx. $6\,\mathrm{m}^2$) could not be weighed. Numerous cameras were used to record the tests, mainly to study the visible flame shape and the smoke spread. In the present paper, an emphasis is put on measuring flame radiative properties, in the visible and infrared domains, as detailed in the next two sections.

2.2. Opacimetry

Opacimetry measurements on a flame are in principle very simple: intensity received from a light source located behind the flame is divided by the intensity measured without the flame. The light source can be polychromatic

and incoherent (e.g. a tungsten halogen source or a blackbody), or monochromatic and coherent (laser). The flame also emits radiation and this emission can reach a high level (and transmission can reach a very low level as will be seen later) if the flame is sooty and thick, which is the case in the present work. Transmitted light has thus to be separated from radiation emitted by the flame itself. Usually this is done by modulating the light with a chopper and demodulating the signal with a lock-in amplifier. These requirements allow to choose the most appropriate light source. Indeed, the spectral intensity emitted by incoherent sources is very small[1], as is the available power in the solid angle of the collecting optics and in the spectral bandwidth of the optical filters[2] used to separate wavelengths and stop most of the radiation emitted by the flame. Moreover, modulating a large area blackbody would be difficult. On the contrary, the spectral intensity emitted by lasers is very high due to their monochromaticity and the very low divergence of their beam. Thus, all the light emitted by a laser (typically a few dozens of milliwatts) is available for the measurement. In addition to that, laser beams can be easily chopped, or even directly modulated. Here, a mechanical chopper at a frequency close to 200 Hz was used (but not equal to 200 Hz in order to avoid a 50 Hz multiple).

In addition to the need to modulate the beams, a second point has to be taken into account: due to refractive index gradients inside the flame, beam deviation is observed (mirage effect). The distance between the emitter and the receiver being equal to several meters, this deviation can reach several centimetres. This is why the light was collected using a 20 cm diameter off-axis parabolic mirror, and focused at the entry of a 150 mm diameter integrating sphere with a 38 mm diameter entry port (see right side in Figure 2). The light coming from all wavelengths was mixed in the integrating sphere: optical band-pass filters were thus used to measure the signal at each wavelength. The light sources were laser diodes, as they are available for many wavelengths, and because they are small enough to be integrated in a compact device. All the laser diodes were thermally stabilised thanks to thermoelectric coolers (TEC), insuring a very stable emission level. Thus, transmission through the flame can be simply calculated by dividing the light intensity during the tests, $I(t)$, by the initial intensity, $I(t = 0)$, measured at the beginning of the experiments. We checked that the signal does not suffer any time drift which could arise from the stability of the laser source or the response of the detectors. This stability is visible in Figure 4 where the signal comes back to its original value at the end of the experiment.

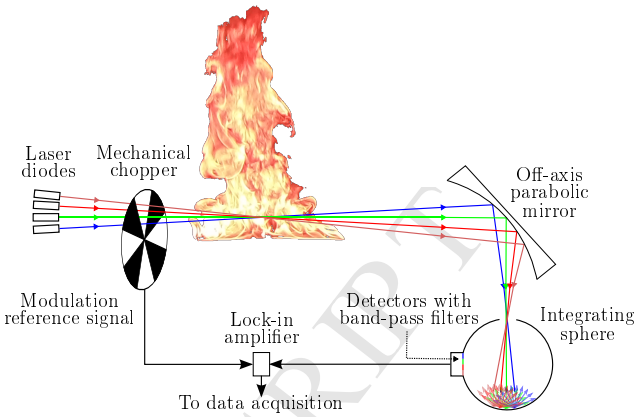

Figure 2: Elements of the opacimetry setup.

Based on this approach, two setups were developed. The first one involved 4 visible and near-infrared wavelengths: 410 nm, 520 nm, 785 nm and 1650 nm. Silicon photodetectors were used for the first three wavelengths, and an InGaAs photodetector was used for the 1650 nm wavelength. The integrating sphere was a Spectralon® sphere suitable for visible and near-infrared wavelengths, up to 2500 nm. The second one involved 4 near-infrared wavelengths: 785 nm, 1650 nm, 2300 nm and 3800 nm. A PbS detector was used for the 2300 nm wavelength, and an InSb detector for the 3800 nm. The integrating sphere was an Infragold® sphere. All the chosen wavelengths are located outside absorption bands of combustion gases so that only soot can significantly absorb at these wavelengths. Measurements were made approximately 10 or 20 cm above the pan (for small or large fires respectively) for the sake of simplicity. Indeed at these heights the flame thickness can be considered equal to the pan diameter. Having a line of sight close to the pool surface could have been a problem because it is likely to cross a fuel-rich atmosphere [29, p. 131], which increases even further the flame inhomogeneity (species and temperature), both in time and space. However, it will be shown that this did not affect the results: the measurements presented here allowed to model the emitted radiation as the emission of an equivalent homogeneous isothermal medium. Photographs of a setup are given in Figure 3.

2.3. Emission spectrometry

For all tests, spectral radiative intensities were measured using a Fourier transform infrared (FTIR) emission spectrometer (Matrix® spectrometer by Bruker®), from 800 cm^{-1} to 6000 cm^{-1} (i.e. 12.5 µm to 1.67 µm). The spectrometer was calibrated with a cavity blackbody (Mikron® model M330EU) at 1200 °C. Measurements were performed at the same height as opacimetry ones (i.e. 10 or 20 cm above the pan), to provide comparable data. Spectral radiation intensities will be used in conjunction with ab-

[1] Peak intensity around 16 $W \cdot m^{-2} \cdot sr^{-1} \cdot nm^{-1}$ for a blackbody at temperature 1000 °C, and 700 $W \cdot m^{-2} \cdot sr^{-1} \cdot nm^{-1}$ for a tungsten halogen source (assuming $T = 2700$ K and emissivity around 0.5 for tungsten).

[2] Assuming a 5×10^{-4} sr^{-1} solid angle and in a 10 nm spectral bandwidth, power is 0.8 mW for a 10×10 cm^2 blackbody, and 20 µW for a 100 W tungsten halogen lamp (assuming a 10 mm^2 emitting surface).

(a) Laser sources (note the green one bouncing off the chopper).

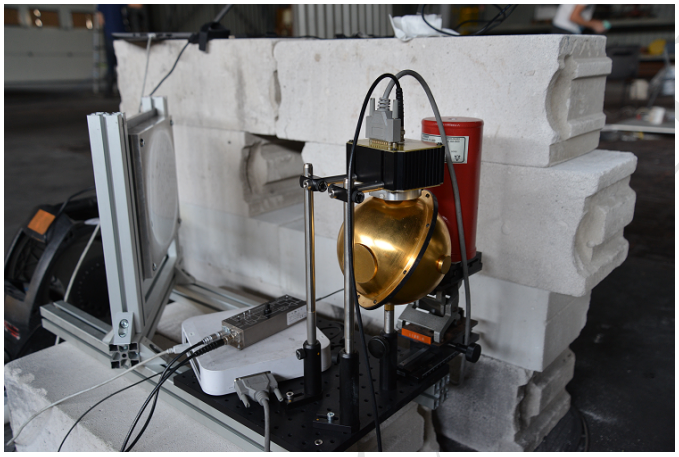

(b) Off-axis parabolic mirror, integrating sphere and detectors.

Figure 3: Opacimetry setup: (a) emission, (b) detection.

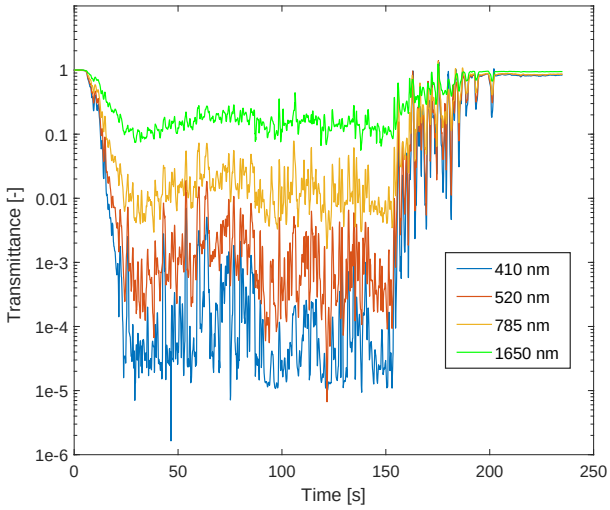

Figure 4: Spectral flame transmittance (log scale) for a 70 cm wide pan at four wavelengths in visible and near-infrared ranges.

sorption coefficients (see Section 3.1) and Equation 3 to compute soot equivalent temperatures T (see Section 3.2).

3. Results

The MLR for large scale experiments (e.g. Figure 1 in [28]) was very stable except at the very beginning and end of the fire. It showed some fluctuations for the small scale experiments because they were carried out with a thiner layer of kerosene and no water. Even so, transmittance and emission measurements always varied around a stable value for the main part of the tests (see Figure 4 for opacimetry), considered here as the steady phase. These results are discussed hereafter.

3.1. Opacimetry

The opacimetry setup allowed to measure transmittance $\mathcal{T}(\lambda_i, t)$ across the flame at various wavelengths λ_i. A typical timeplot is shown in Figure 4 for a 70 cm wide fire. The presence of the flame during combustion is clearly visible, with a very large decrease in transmittance for all wavelengths and especially for the smallest ones. The differences in attenuation from one wavelength to another are particularly obvious (i.e. non-grey transmittance). For the smallest wavelength, transmittance levels down to a few 10^{-5} could be measured.

3.1.1. Mean optical thickness

Transmittance measurements can be converted to optical thicknesses according to

$$\tau(\lambda_i) = -\ln\left(\mathcal{T}(\lambda_i)\right). \tag{4}$$

For each test, mean optical thicknesses were calculated over the steady phase. Only one repeat was usable for the

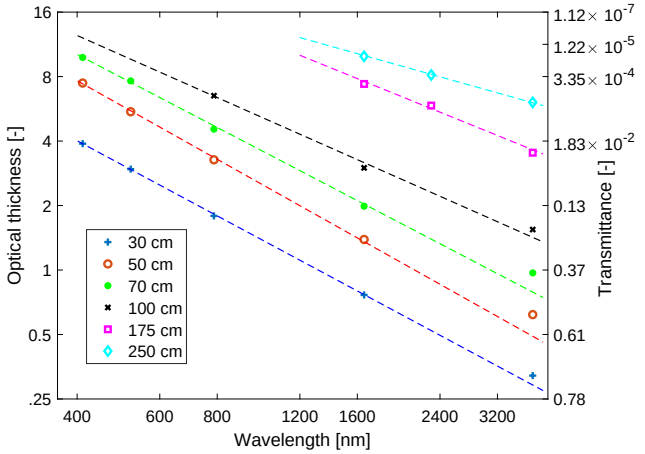

Figure 5: Mean optical thickness as a function of wavelength for various fire sizes, in log-log base 2 scale.

largest fires (pan widths of 250 cm, 175 cm and 100 cm) performed in the ADP aircraft hangar. For smaller fires (widths from 70 cm to 30 cm) performed in the PROMETHEI facility, several test results could be used for each size. The values presented in Figure 5 are thus a weighted average of the mean optical thickness for each test, with a weight proportional to the steady phase duration.

We can see in Figure 5 that optical thickness increases with flame width. Short wavelengths were not used for large fires because transmittance would have been negligible (very large optical thickness). With the log-log scale used in Figure 5, the graphs representing the optical thickness versus wavelength follow straight lines, which is in agreement with the power law $\kappa(\lambda) = C f_v / \lambda^\alpha$ mentioned in the introduction (see Equation 2 and Reference [19]). The slope α is around -1.15 for fire widths less than or equal to 70 cm. Above this size, the larger the fire, the smaller the slope. It is difficult to state if this decrease has a physical meaning, or if it is a measurement artifact due to the very low transmittance values (see Figure 5, right axis). Indeed, such values are close to the noise level of the infrared detectors, and close to the ability of the lock-in detection to remove the high level of radiation emitted by the flame itself in the infrared domain. Thus, "true" transmission for these fire sizes could be lower than the measured values (i.e. larger optical thickness), and actual slopes could thus be higher.

3.1.2. Flame extinction coefficient

As seen in Figure 4, transmittance fluctuates significantly with time due to the turbulent nature of the flames investigated here. Transmission levels also vary a little from one test to another, because experimental conditions cannot be exactly the same for each test. For these reasons, time-resolved analyses of the transmission were performed, in order to obtain mean and standard deviation values of the results for each test.

FTIR spectra are usually presented as functions of wavenumber[3], generally expressed in cm^{-1}, which is the inverse of the wavelength ($\sigma = 1/\lambda$). For this reason wavenumbers will be used instead of wavelengths in the following. Moreover, the power law mentioned earlier to describe the spectral dependence of $\kappa(\lambda)$ (see Equation 2) and $\tau(\lambda)$ (see Section 3.1.1) is rewritten as

$$\frac{\tau(\sigma)}{\ell} = \beta(\sigma) = \beta_0 \left(\frac{\sigma}{\sigma_0} \right)^\alpha, \qquad (5)$$

where β_0 is the extinction coefficient at a reference wavenumber σ_0 (here $\sigma_0 = 4000\,\mathrm{cm}^{-1}$ was chosen, i.e. $\lambda_0 = 2.5\,\mu\mathrm{m}$). This allows to use the dimensionless term σ/σ_0, which is preferable with the non-integer exponent α. Optical thickness was divided by the geometrical thickness of the flame, assumed to be equal to the pan size ℓ (as measurements were performed near the base of the flame) in order to obtain an equivalent extinction coefficient $\beta(\sigma)$. For each test, the extinction coefficient was fitted with the model in Equation 5. In this way, time variations of β_0 and α were obtained. Means and standard deviations of β_0 and α are represented in Figure 6. The extinction coefficient β_0 is around $1.74\,\mathrm{m}^{-1}$ for flame thicknesses from 30 cm to 70 cm. For wider flames, β_0 increases to $2.1\,\mathrm{m}^{-1}$ for the 100 cm thick flame, and to $3.1\,\mathrm{m}^{-1}$ for the 175 and 250 cm thick flames. Such an increase could be expected as the soot volume fraction is likely to increase for large flames. Even so, variations of the extinction coefficient are small for flames thinner or equal to 70 cm, and remain moderate for thicker flames. This is an interesting feature which is a benefit of the flame volume model over a surface model. Indeed, for the latter, emissivity (e.g. ϵ in Equation 1) has to be strongly dependent on the flame thickness. Regarding the exponent α, it is around 1.12 for tests with a width less than or equal to 70 cm. Above this size, the exponent decreases, as already seen in Figure 5. Whether these smaller values of α have a physical meaning or not is not determined yet (as discussed for the slope α in Section 3.1.1).

3.2. Spectrometry

An example of emission spectra is shown in Figure 7 for a 50 cm wide flame. The spectral resolution is equal to $4\,\mathrm{cm}^{-1}$. A total of 40 spectra are presented, each spectrum being acquired every 2.5 s. Acquisition time[4] of a spectrum is about 0.2 s, which is smaller than the flame pulsation period. The spectrum acquisition rate was not

[3] Wavenumbers appear naturally in FTIR spectroscopy because they are the reciprocal quantity of the interferogram optical path difference. Thus FTIR spectra have equally spaced points when expressed in wavenumbers. Incidentally, this makes easier spectra integration if needed.

[4] Acquisition time of the full interferogram allowing the $4\,\mathrm{cm}^{-1}$ resolution. Information required for a $100\,\mathrm{cm}^{-1}$ resolution allowing a good enough spectrum outside gases emission wavelength bands is contained in less than 5 ms around the interferogram center-burst.

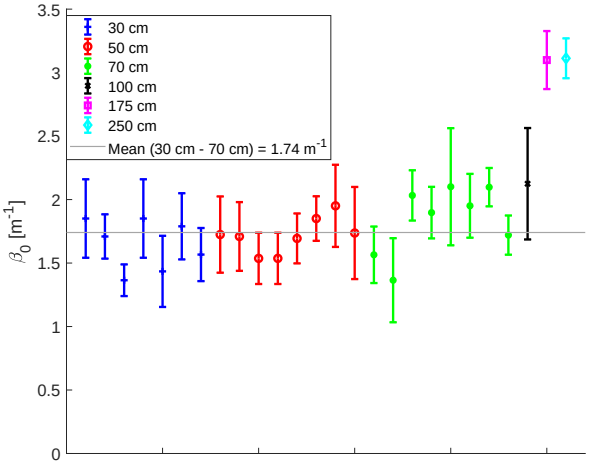

(a) Extinction coefficient β_0.

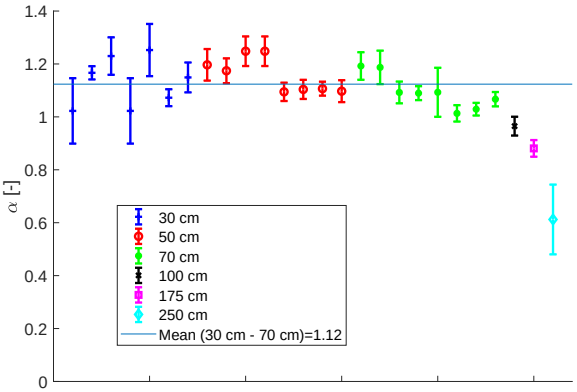

(b) Exponent α.

Figure 6: Parameters of Equation 5 for all fire sizes (several repeats for the smaller ones).

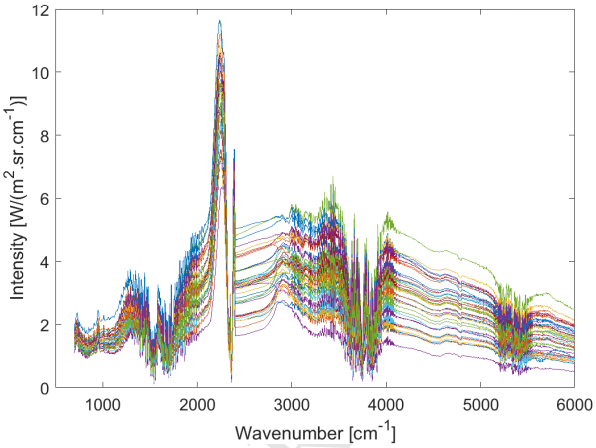

Figure 7: Examples of "instantaneous" spectra for a 50 cm wide flame.

sufficiently high to resolve time variations of the emitted radiation due to the flame turbulence and pulsation. As a consequence, the intensity measured by the spectrometer undergoes large and apparently random time variations. These variations are further amplified because measurements are made across the fuel-rich region of the flame, which is strongly affected by the flame pulsation. It can be pointed out that spectra with a small intensity (low temperature and/or low soot optical thickness) are associated with a high emission level by hydrocarbon vapours, seen around 2900 cm^{-1}. Yet, such a time resolved characterisation of the emitted radiation was not the goal of the present work. We focused instead on averaged data. In a first step, analyses were performed on spectra averaged over all the flame steady phase (see Section 3.2.1). Later, complementary investigations were conducted on "instantaneous" spectra (see Section 3.2.2) in order to check if data (i.e. extinction coefficient and equivalent temperature) extracted from averaged spectra give similar results than averaged data calculated from "instantaneous" spectra.

3.2.1. Mean spectra

Considering the emission of radiation by a homogeneous and isothermal equivalent medium, as proposed in the introduction, the intensity is given by

$$I_\sigma(s=e) = \left(1 - \exp\left(-\kappa(\sigma)e\right)\right) I_\sigma^{\mathrm{bb}}(T). \quad \text{(see 3)}$$

As already discussed, I_σ depends on $\kappa(\sigma)$ and T. For the infrared wavelengths involved here, soot scattering can be considered negligible, as explained in Appendix A. Thus the absorption coefficient $\kappa(\sigma)$ is equal to the extinction coefficient $\beta(\sigma)$ previously determined through opacimetry measurements. As averaged spectra are considered, a mean absorption coefficient is used. It was shown in Section 3.1.2 that the extinction coefficient, and thus the absorption

coefficient, can be well approximated by

$$\kappa(\sigma) = \beta_0 \left(\frac{\sigma}{\sigma_0}\right)^{\alpha}. \quad (6)$$

Combining Equations 3 and 6 thus gives

$$I_\sigma(s=e) = \left(1 - \exp\left[-\beta_0 \left(\frac{\sigma}{\sigma_0}\right)^{\alpha} e\right]\right) I_\sigma^{\mathrm{bb}}(T). \quad (7)$$

This model is a three-parameter model: β_0, α and T have to be determined. The exponent α was found to be almost constant for flames thinner or equal to 70 cm (see Figure 6(b)), and it decreases for larger flames. Whether or not this variation has a physical meaning still has to be investigated (see discussion in Section 3.1.1), but ignoring it for the present study is considered a reasonable approximation. Indeed, as the fire gets wider (e increases in Equation 3), the flame becomes optically thicker and its emission tends towards that of a blackbody ($\exp(-\kappa(\sigma)e) \to 0 \implies I_\sigma(s=e) \to I_\sigma^{\mathrm{bb}}(T)$). In this limit, the radiation intensity I_σ thus becomes insensitive to the variations of the absorption coefficient or the parameters used to compute it. For this reason, a constant α was deemed acceptable. A slight correction was made to the value presented earlier (in Section 3.1.2, where $\alpha = 1.12$), because it was determined over the whole range of wavelengths used for opacimetry (i.e. 410 nm to 3800 nm), and not only for the infrared range. It is observed in Figure 5 that the agreement between the modelled mean extinction coefficient and the measured values is poorer for infrared wavelengths. In order to use Equation 6 in conjunction with spectrometry measurements (performed from 2000 nm to 12 500 nm), a new fit was performed using only infrared values, resulting in $\alpha = 1.07$. Regarding β_0 (extinction coefficient at the reference wavenumber $\sigma_0 = 4000\,\mathrm{cm}^{-1}$), it was shown in Section 3.1.2 that β_0 is almost independent of flame thickness (see Figure 6(a)), with $\beta_0 \approx 1.74\,\mathrm{m}^{-1}$ for flame thicknesses less or equal to 70 cm, $\beta_0 \approx 2.1\,\mathrm{m}^{-1}$ for the 100 cm thick flame, and $\beta_0 \approx 3.1\,\mathrm{m}^{-1}$ for 175 and 250 cm thick flames. For this first analysis, which uses averaged spectra, β_0 was fixed to one of these mean values obtained from opacimetry measurements, depending on flame thickness. Hence, T is the only remaining unknown. This equivalent temperature was determined by adjusting the model in Equation 7 to the experimental spectra. We call this model the "one-parameter model", as α was fixed to 1.07, and β_0 to one of the three values listed above, depending on flame thickness. The adjustment was done with the `nlinfit` Matlab® function, over the spectral ranges $[2430 - 2700]$ cm^{-1}, $[4185 - 4340]$ cm^{-1} and $[4650 - 5030]$ cm^{-1}. These values were chosen because they are outside emission bands of combustion gases, and absorption bands of atmospheric gases located between the flame and the spectrometer. Indeed, the model presented here focuses on radiation by soot: emission and absorption by gases are not taken into account. The latter will be accounted for in the future, with a Statistical Narrow Band (SNB) or a Correlated-k (Ck) approach [30] for example.

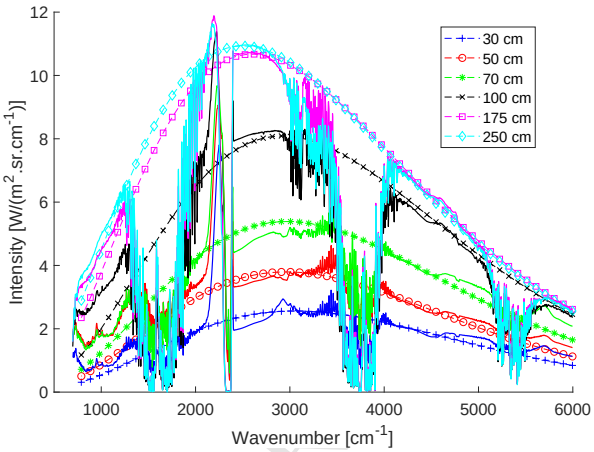

Figure 8: Mean emission spectra for all fire sizes, and the adjustments using the one-parameter model (i.e. Equation 7 with α and β_0 fixed).

Typical mean emission spectra and their adjustments are shown in Figure 8 for all fire sizes. We see that a quite good agreement is obtained outside combustion gases emission bands and atmospheric gases absorption bands. Note that atmospheric gases absorption is particularly high for large size fires, as spectrometry measurements at the ADP hangar were performed 23 m away from the fire. For tests performed in the PROMETHEI facility, the distance was only 4 m, and thus absorption is less pronounced. The agreement is poorer for large wavelengths (above 4 µm, i.e. wavenumbers below 2500 cm^{-1}). This could show a limit of the power law used to describe spectral variations of the absorption coefficient (e.g. Equation 2 or Equation 6). Indeed, this model was considered valid over the entire spectral range investigated here, but there is no experimental validation for large wavelengths. It is worth mentioning that, although the results of the model may resemble blackbody curves, only very thick flames can indeed be computed using Planck's law, with emissivities close to unity. All other flames cannot be modelled as blackbodies or grey bodies, that is using constant (non-wavelength-dependent) emissivities. A given grey body could describe the data for short wavelengths but not large ones, and another one could do the opposite, but no grey body can describe the radiation intensity over the entire spectrum, and thus the spectral energy distribution.

The temperature identified for the various tests at different sizes is shown in Figure 9. The average temperature is 1208 K. Although values fluctuate around this mean, no clear trend can be linked to flame thickness. This temperature can thus be considered an intrinsic characteristic of kerosene flames.

3.2.2. Instantaneous spectra

As seen in Figure 7, emission spectra show some large variations with time as a consequence of the pulsation and the turbulence of the flame. These changes are undoubtedly due to variations of both the optical thickness

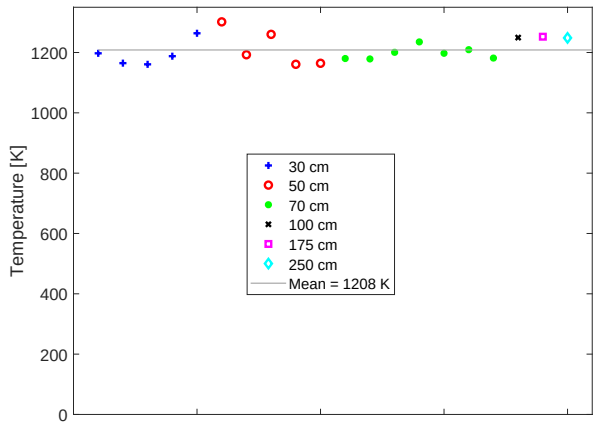

Figure 9: Identified temperatures from adjustments made on mean spectra using the one-parameter model (i.e. Equation 7 with α and β_0 fixed).

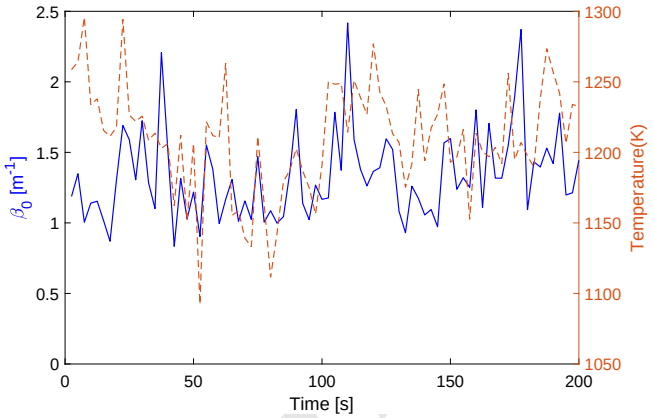

Figure 10: Temperature T and extinction coefficient β_0 identified from adjustments on "instantaneous" spectra using the two-parameter model (i.e. Equation 7 with α fixed). Flame thickness equal to 50 cm.

and the temperature of the flame. In the previous section, results where time-averaged over the steady phase of the fire (e.g. mean optical thicknesses in Section 3.1.2 and averaged spectra in Section 3.2.1). In order to apply the model in Equation 7 to instantaneous spectra, time-resolved parameters are now needed. Theoretically, a fit would have been possible by keeping free all parameters (β_0, α and T). However, this produced non-physical results, with high or low values of β_0 and α, due to a correlation between these two coefficients. It was thus chosen to keep only two parameters free (β_0 and T), and to fix the value for α. The latter was held constant ($\alpha = 1.07$), as this coefficient is intrinsic to soot properties (optical index and size distribution), and time variations of this parameter can be considered negligible. The dispersion shown by the error bars in Figure 6(b) is probably due to the measurement process. Indeed, the laser beams are not perfectly coaxial, and so they do not follow exactly the same path inside the flame. This means that part of the transmittance difference between two wavelengths is in fact due to spatial variation of the extinction coefficient, and not to a spectral variation. Keeping a constant value for α is therefore considered to be a reasonable assumption. On the contrary, time variations of β_0 are very likely due to large changes of soot concentration in space and time. Time and space variations of temperature are also certain. To summarise, fits of instantaneous spectra were performed with the model in Equation 7, with two free parameters (β_0 and T), and α being fixed to 1.07. This two-parameter adjustment was performed only for flame thicknesses less than or equal to 100 cm. This is because for larger fires, and for the spectral range in which the adjustment is made, the emitted radiation approaches that of a blackbody, and thus the model becomes insensitive to the extinction coefficient (or to the exponent α as discussed in Section 3.2.1). Therefore, for the 175 and 250 cm wide flames, the "instantaneous" spectra were adjusted with the one-parameter model described earlier (see Section 3.2.1), with fixed values of α and β_0 derived from opacimetry measurements. Thus, only the flame temperature was identified for these two large fire sizes. An example of result with the two-parameter model is shown in Figure 10 for a 50 cm thick flame.

From the time variation of β_0 and T obtained for several tests with flame size varying from 30 cm to 100 cm, means and standard deviations were calculated and are shown in Figure 11. It can be seen that the identified β_0 varies very little with the flame size from 30 cm to 70 cm, and increases for the 100 cm thick flame, similarly to what was observed in Section 3.1.2. For thin flames, the mean value of β_0 is approximately 1.44 m^{-1}, which is smaller but close to the result obtained previously from opacimetry measurements (i.e. $\beta_0 = 1.74\,\mathrm{m}^{-1}$). As for the temperature, a mean value equal to 1243 K was identified, with no clear variation with the flame size, as was already observed in Section 3.2.1. Typical standard deviation is around 30 K. The average temperature is slightly higher than the one obtained with the one-parameter model (1208 K), which is related to the smaller extinction coefficients identified here. Indeed, for a given intensity, a decrease in extinction coefficient is linked to an increase in temperature. It is remarkable to see that the temperature dispersion around the mean value is significantly reduced compared to the one in Figure 9. This is a benefit of the two-parameter model, compared to the one-parameter model, because the extinction coefficient (or equivalently the optical thickness) of the flame is allowed to vary and to better estimate the actual value.

Two-parameter fits were also performed on averaged spectra. An example for each flame thickness from 30 cm to 100 cm is shown in Figure 12. The fit is significantly improved compared to the fit obtained with the one-parameter model (Figure 8). The extinction coefficients β_0 and tem-

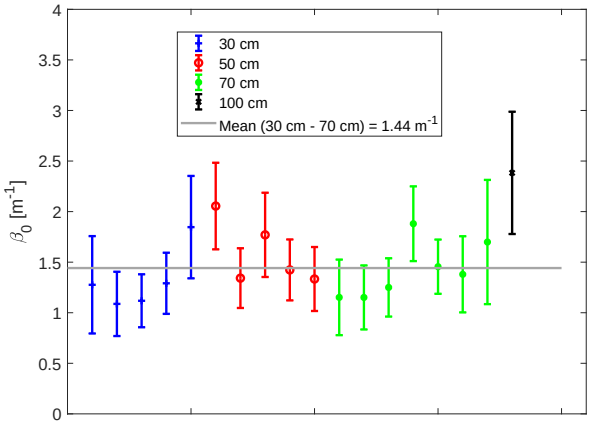

(a) Extinction coefficient β_0. The mean value (horizontal line) is based on results for fire widths less than or equal to 70 cm.

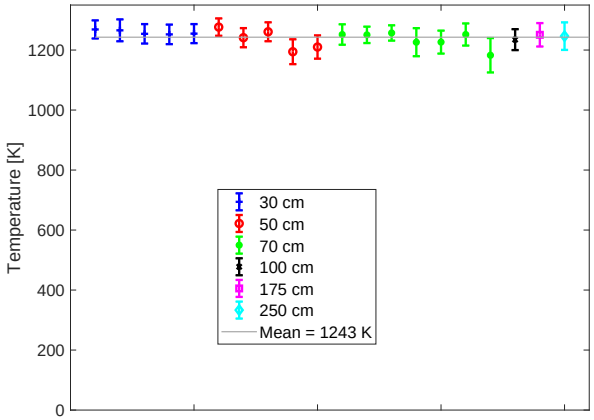

(b) Temperature T. The mean value (horizontal line) is based on all results.

Figure 11: Parameters of Equation 7 for all fire sizes (several repeats for the smaller ones).

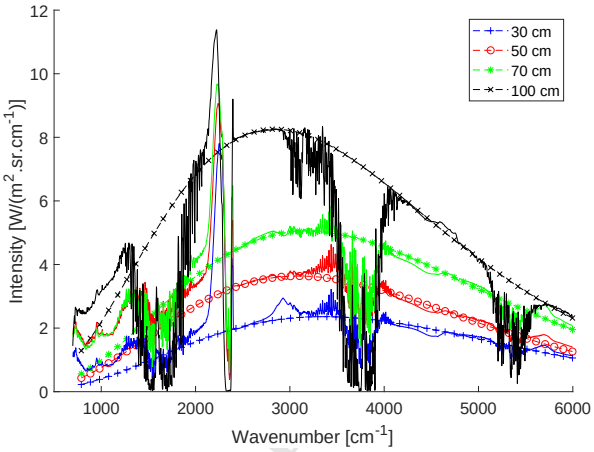

Figure 12: Mean emission spectra for fire width up to 100 cm, and the adjustments using the two-parameter model (i.e. Equation 7 with α fixed).

peratures T using the two-parameter approach on averaged spectra are remarkably close to the mean values identified by fitting each individual "instantaneous" spectrum: the largest differences were 2% for β_0 and 4 K for T. This shows that analyses on averaged spectra provide reliable mean values for the extinction coefficient and the temperature. This means that, although the average of Planck functions at different temperatures is not mathematically equal to the Planck function at the average temperature, in practice there is little difference between the two calculations. This means that if only average values are sought it is possible to work with averaged spectra, which is faster and simpler than a spectrum by spectrum approach. The latter is useful to get additional information, mainly standard deviations.

4. Conclusions

In order to describe radiation from soot in flames, a model considering an equivalent homogeneous isothermal medium was presented. Its key parameters, namely an equivalent absorption coefficient and an equivalent temperature, were determined for kerosene using data acquired through an extensive experimental campaign (square pool fires, widths from 30 cm to 250 cm). The two measurement techniques used to characterise these optical properties were described (see Section 2). The visible and near-infrared opacimetry setups produced transmittance values at multiple wavelengths, which allowed to determine the absorption coefficients in the form of a power law (see Equation 6) using two parameters, namely extinction coefficients β_0 and exponents α. Using these values and the infrared spectrometry measurements, the equivalent temperatures could be computed (see Section 3.2). All these parameters (i.e. β_0, α and T) were found to be almost independent of flame size. Using averaged spectra was shown to provide comparable values to a spectrum

by spectrum analysis. More generally, the results prove that spectrally resolved measurements are a valuable investment when studying flames, and that further work is still needed to accurately model them.

In addition to kerosene, other fuels (wood, heptane, diesel and polyurethane foam) are being investigated. The optical properties presented here will also be used in conjuction with flame geometry measurements to model radiation, and compare the results to the heat fluxes recorded during the tests.

Another key aspect that could not be addressed so far is flame inhomogeneity: complementary tests could be performed to produce "radiative maps" of flames, as done before [14, 15, 31] but with the multispectral approach presented here (e.g. [22]). A first step would be to conduct the measurements presented here (i.e. opacimetry and emission spectrometry) along the flame centerline at various heights. These additional data would also confirm if the line of sight used in the present study can be considered representative of the flame volume that is being modelled [12, 22].

To conclude, the model presented here offers an analytical formulation to account for the spectral dependence of soot radiation, and thus provides a more detailed description of flames while being computationally efficient. As the key parameters appear to be independent of flame size, only a few tests would be required to determine their values and produce a database for several fuels. An example of end application is to provide a detailed description of heat transfers for fire spread models, meant to predict full-scale burning behaviour based on small-scale tests.

Declarations of interest

None.

Acknowledgements

The authors would like to thank the staff of the Fire Engineering division at LCPP for performing the large scale tests, and more widely all personnel of the Préfecture de Police who helped setting them up. Groupe ADP is once again acknowledged for providing the test site. The technical staff at LEMTA is thanked for designing and building measuring devices and other equipment.

Funding: This work was supported by the Laboratoire Central de la Préfecture de Police and the Laboratoire Énergies et Mécanique, Théorique et Appliquée (UMR 7563, Université de Lorraine/CNRS).

Appendix A. Assessment of soot scattering

This appendix is meant to explain why soot scattering in the infrared was neglected, allowing to consider that the absorption coefficient $\kappa(\lambda)$ is nearly equal to the measured extinction coefficient $\beta(\lambda)$.

Soot particles are recognised for years to be pseudo-fractal aggregates of primary carbonaceous spherical particles. The number of primary particles follows the law [32]

$$N = k_\mathrm{f} \left(\frac{R_\mathrm{g}}{d_\mathrm{p}} \right)^{D_\mathrm{f}}, \tag{A.1}$$

where d_p is the diameter of primary particles, R_g the gyration radius, D_f the fractal dimension and k_f the prefactor parameter of the aggregate. The Rayleigh Debye Gans theory for Fractal Aggregates (RDG-FA) is nowadays the most used theory to describe the interaction between light and soot. The review by Sorensen [32] presents in details soot properties and the RDG-FA.

According to this theory, the absorption cross section is given by

$$\sigma_\mathrm{abs} = N 4\pi k \, R_\mathrm{p}^3 \, E(m), \tag{A.2}$$

whereas the scattering cross section is given by

$$\sigma_\mathrm{sca} = N^2 \, \frac{8\pi}{3} \, k^4 \, R_\mathrm{p}^6 \, F(m) \, g(kR_\mathrm{g}), \tag{A.3}$$

where $R_\mathrm{p} = d_\mathrm{p}/2$, $k = 2\pi/\lambda$, $E(m) = \mathrm{Im}\left(\frac{m^2-1}{m^2+1}\right)$, $F(m) = \left|\frac{m^2-1}{m^2+1}\right|^2$, m being the complex optical index of soot, and $g(kR_\mathrm{g})$ the total scattering form factor.

As pointed out by Krishnan *et al.* [33], the ratio ρ_sa between scattering and absorption is given by

$$\rho_\mathrm{sa} = \frac{2}{3} N \, (kR_\mathrm{p})^3 \, g(kR_\mathrm{g}) \, \frac{F(m)}{E(m)}. \tag{A.4}$$

As a consequence, the bigger the aggregate (large N), the higher ρ_sa. Regarding spectral variations, ρ_sa is proportional to $(kR_\mathrm{p})^3 = 8\pi^3 \, (R_\mathrm{p}/\lambda^3)$. Thus, the smaller the particle or the larger the wavelength, the lower the scattering/absorption ratio. The last parameter is the $F(m)/E(m)$ ratio. Krishnan *et al.* report measurements of this parameter by several groups as well as their own, up to infrared wavelengths. The spectral trend of this ratio is a clear increase with wavelength. Overall, spectral variations of ρ_sa are a competition between the decrease with λ due to the $(kR_\mathrm{p})^3$ term and an increase due to the $F(m)/E(m)$ ratio. Because of the cubic dependence, the first factor ends up always winning. Using measured soot morphologies and inferred soot optical indices, Krishnan *et al.* calculate estimates of ρ_sa ratios for various fuels as a function of wavelength from visible to infrared. Kerosene soot is not referenced in this paper. A maximum, between 0.35 and 0.7 depending on the fuel, is observed at a wavelength around 500 nm. Beyond this maximum, ρ_sa decreases rapidly.

Regarding the present work, infrared spectra begin at 1.67 µm, and the main wavelength range is beyond 2 µm. For this wavelength, the maximum value of ρ_sa is equal to 0.15, for benzene soot [33]. The parameter used to quantify scattering is usually the single scattering albedo $\omega = \sigma_\mathrm{sca}/\sigma_\mathrm{ext} = \sigma_\mathrm{sca}/(\sigma_\mathrm{sca} + \sigma_\mathrm{abs})$ which is related to ρ_sa

by $\omega = \rho_{sa}/(1+\rho_{sa})$. Thus, a ratio $\rho_{sa} = 0.15$ corresponds to a 0.13 albedo, whereas the ρ_{sa} maximum values (between 0.35 and 0.7) correspond to albedos between 0.26 and 0.41 respectively. Bond and Bergstrom [34] report albedos determined by various groups to be in the range 0.15–0.29, with most values below 0.2, for wavelengths in the range 514 nm to 633 nm, which is significantly smaller than the values measured and estimated by Krishnan *et al.* Moreover, the measurements of Krishnan *et al.* were performed overfire, whereas ours are performed in-fire, and even near the pool surface. Krishnan *et al.* reported that in-fire soot particles are significantly smaller (N in the range 30–80) than overfire soot (N in the range 420–550, excluding n-heptane [$N = 260$], known to produce small size soot). As ρ_{sa} is linearly related to N, a decrease in soot size leads to a decrease in scattering. Soot morphology of in-fire and overfire 2-meter wide JP-8 kerosene pool fires was studied by Jensen *et al.* [35]. Reported primary particles diameters are in the range 57 nm–74 nm and gyration radii between 239 and 340 nm. Corresponding primary particle number N calculated by Equation A.1 are in the range 55–95, which is significantly smaller than the values determined in the paper by Krishnan *et al.* and implies consequently less scattering. Regarding primary particles, Huang *et al.* [36] recently reported primary particle diameter of kerosene soot (sampled in and over the flame of a small pool pan) in the range 50 nm to 60 nm, which is somewhat smaller than the values of Jensen *et al.*

As a conclusion, the highest reported scattering albedo for the infrared spectral range under consideration in the present work, that is wavelengths higher than 2 µm, is $\omega = 0.15$ [33]. The value for in-fire kerosene soot is likely to be significantly smaller, owing to smaller soot aggregates sizes and albedos reported in other works [34–36]. Moreover the albedo, and thus scattering, decrease very fast with increasing wavelengths. This is why scattering by soot particles was neglected in the infrared spectral range considered here.

References

[1] V. Babrauskas, Estimating large pool fire burning rates, Fire Technology 19 (4) (1983) 251–261. doi:10.1007/BF02380810.

[2] A. C. Fernandez-Pello, T. Hirano, Controlling Mechanisms of Flame Spread, Combustion Science and Technology 32 (1-4) (1983) 1–31. doi:10.1080/00102208308923650.

[3] X. Silvani, F. Morandini, Fire spread experiments in the field: Temperature and heat fluxes measurements, Fire Safety Journal 44 (2) (2009) 279–285. doi:10.1016/j.firesaf.2008.06.004.

[4] V. C. Raj, S. V. Prabhu, A refined methodology to determine the spatial and temporal variation in the emissivity of diffusion flames, International Journal of Thermal Sciences 115 (2017) 89–103. doi:10.1016/j.ijthermalsci.2017.01.016.

[5] J. R. Beyreis, H. W. Monsen, A. F. Abbasi, Properties of wood crib flames, Fire Technology 7 (2) (1971) 145–155. doi:10.1007/BF02588954.

[6] A. Àgueda, E. Pastor, Y. Pérez, E. Planas, Experimental study of the emissivity of flames resulting from the combustion of forest fuels, International Journal of Thermal Sciences 49 (3) (2010) 543–554. doi:10.1016/j.ijthermalsci.2009.09.006.

[7] P. H. Thomas, Rates of Spread of Some Wind-driven Fires, Forestry: An International Journal of Forest Research 44 (2) (1971) 155–175. doi:10.1093/forestry/44.2.155.

[8] C. Qian, K. Saito, Measurements of pool-fire temperature using IR technique, in: Combustion Fundamentals and Applications: Joint Technical Meeting Proceedings, San Antonio, USA, 1995, pp. 81–86.

[9] E. Den Breejen, M. Roos, K. Schutte, J. De Vries, J. Winkel, Infrared Measurements of Energy Release and Flame Temperatures of Forest Fires, in: D. Viegas (Ed.), Proceedings of the 3rd Int. Conf. on Forest Fire Research, ADAI - Associacao para o Desenvolvimento da Aerodinamica Industrial, Coimbra, Portugal, 1998, pp. 517–553.

[10] E. Pastor, A. Rigueiro, L. Zárate López, A. Giménez, J. Arnaldos Viger, E. Planas Cuchi, Experimental methodology for characterizing flame emissivity of small scale forest fires using infrared thermography techniques, in: D. Viegas (Ed.), Proceedings of the 4th Int. Conf. on Forest Fire Research, Millpress, Rotterdam, Netherlands, Coimbra, Portugal, 2002, pp. 1–11.

[11] E. Planas-Cuchi, J. M. Chatris, C. López, J. Arnaldos, Determination of Flame Emissivity in Hydrocarbon Pool Fires Using Infrared Thermography, Fire Technology 39 (3) (2003) 261–273. doi:10.1023/A:1024193515227.

[12] J.-L. Dupuy, P. Vachet, J. Maréchal, J. Meléndez, A. J. d. Castro, Thermal infrared emission–transmission measurements in flames from a cylindrical forest fuel burner, International Journal of Wildland Fire 16 (3) (2007) 324–340. doi:10.1071/WF06043.

[13] S. Sudheer, S. V. Prabhu, Measurement of flame emissivity of gasoline pool fires, Nuclear Engineering and Design 240 (10) (2010) 3474–3480. doi:10.1016/j.nucengdes.2010.04.043.

[14] S. Sudheer, S. V. Prabhu, Measurement of Flame Emissivity of Hydrocarbon Pool Fires, Fire Technology 48 (2) (2012) 183–217. doi:10.1007/s10694-010-0206-5.

[15] V. C. Raj, S. V. Prabhu, Measurement of geometric and radiative properties of heptane pool fires, Fire Safety Journal 96 (2018) 13–26. doi:10.1016/j.firesaf.2017.12.003.

[16] H.-C. Zhou, C. Lou, Q. Cheng, Z. Jiang, J. He, B. Huang, Z. Pei, C. Lu, Experimental investigations on visualization of three-dimensional temperature distributions in a large-scale pulverized-coal-fired boiler furnace, Proceedings of the Combustion Institute 30 (1) (2005) 1699–1706. doi:10.1016/j.proci.2004.08.090.

[17] H. Liu, S. Zheng, H. Zhou, C. Qi, Measurement of distributions of temperature and wavelength-dependent emissivity of a laminar diffusion flame using hyper-spectral imaging technique, Measurement Science and Technology 27 (2) (2016) 025201. doi:10.1088/0957-0233/27/2/025201.

[18] M. Sibulkin, Estimates of the Effect of Flame Size on Radiation from Fires, Combustion Science and Technology 7 (3) (1973) 141–143. doi:10.1080/00102207308952352.

[19] M. F. Modest, Radiative Properties of Particulate Media, in: M. F. Modest (Ed.), Radiative Heat Transfer, third edition Edition, Academic Press, Boston, USA, 2013, pp. 387–439. doi:10.1016/B978-0-12-386944-9.50012-1.

[20] T. Steinhaus, S. Welch, R. O. Carvel, J. L. Torero, Large-scale pool fires, Thermal Science 11 (2) (2007) 101–118.

[21] K. Wakatsuki, G. S. Jackson, A. Hamins, M. R. Nyden, Effects of fuel absorption on radiative heat transfer in methanol pool fires, Proceedings of the Combustion Institute 31 (2) (2007) 2573–2580. doi:10.1016/j.proci.2006.08.049.

[22] J. M. Suo-Anttila, T. K. Blanchat, A. J. Ricks, A. L. Brown, Characterization of thermal radiation spectra in 2m pool fires, Proceedings of the Combustion Institute 32 (2) (2009) 2567–2574. doi:10.1016/j.proci.2008.06.044.

[23] T. Sikanen, S. Hostikka, Modeling and simulation of liquid pool fires with in-depth radiation absorption and heat transfer, Fire Safety Journal 80 (2016) 95–109. doi:10.1016/j.firesaf.2016.01.002.

[24] G. Linteris, M. Zammarano, B. Wilthan, L. Hanssen, Absorption and reflection of infrared radiation by polymers in fire-

like environments, Fire and Materials 36 (7) (2012) 537–553. doi:10.1002/fam.1113.

[25] P. Boulet, J. Gérardin, Z. Acem, G. Parent, A. Collin, Y. Pizzo, B. Porterie, Optical and radiative properties of clear PMMA samples exposed to a radiant heat flux, International Journal of Thermal Sciences 82 (2014) 1–8. doi:10.1016/j.ijthermalsci.2014.03.013.

[26] G. Parent, Z. Acem, S. Lechêne, P. Boulet, Measurement of infrared radiation emitted by the flame of a vegetation fire, International Journal of Thermal Sciences 49 (3) (2010) 555–562. doi:10.1016/j.ijthermalsci.2009.08.006.

[27] P. Boulet, G. Parent, Z. Acem, A. Kaiss, Y. Billaud, B. Porterie, Y. Pizzo, C. Picard, Experimental Investigation of Radiation Emitted by Optically Thin to Optically Thick Wildland Flames, Journal of Combustion 2011 (2011) 137437. doi:10.1155/2011/137437.

[28] G. Erez, G. Parent, A. Collin, P. Boulet, M. Suzanne, E. Faure, Aurélien Thiry-Muller, Flame properties of large kerosene fires, Journal of Physics: Conference Series 1107 (4) (2018) 042035. doi:10.1088/1742-6596/1107/4/042035.

[29] S. R. Tieszen, T. J. O'Hern, E. J. Weckman, R. W. Schefer, Experimental study of the effect of fuel mass flux on a 1-m-diameter methane fire and comparison with a hydrogen fire, Combustion and Flame 139 (1) (2004) 126–141. doi:10.1016/j.combustflame.2004.08.006.

[30] V. P. Solovjov, B. W. Webb, F. André, Radiative Properties of Gases, in: F. A. Kulacki (Ed.), Handbook of Thermal Science and Engineering, Springer International Publishing, Cham, 2017, pp. 1–74. doi:10.1007/978-3-319-32003-8_59-1.

[31] G. H. Markstein, Scanning-radiometer measurements of the radiance distribution in PMMA pool fires, Symposium (International) on Combustion 18 (1) (1981) 537–547. doi:10.1016/S0082-0784(81)80059-8.

[32] C. M. Sorensen, Light Scattering by Fractal Aggregates: A Review, Aerosol Science and Technology 35 (2) (2001) 648–687. doi:10.1080/02786820117868.

[33] S. S. Krishnan, K.-C. Lin, G. M. Faeth, Extinction and Scattering Properties of Soot Emitted From Buoyant Turbulent Diffusion Flames, Journal of Heat Transfer 123 (2) (2000) 331–339. doi:10.1115/1.1350823.

[34] T. C. Bond, R. W. Bergstrom, Light Absorption by Carbonaceous Particles: An Investigative Review, Aerosol Science and Technology 40 (1) (2006) 27–67. doi:10.1080/02786820500421521.

[35] K. A. Jensens, J. M. Suo-Anttila, L. G. Blevins, Measurement of Soot Morphology, Chemistry, and Optical Properties in the Visible and Near-Infrared Spectrum in the Flame Zone and Overfire Region of Large Jp-8 Pool Fires, Combustion Science and Technology 179 (12) (2007) 2453–2487. doi:10.1080/00102200701484266.

[36] D. Huang, C. Guo, L. Shi, Experimental investigation on the morphology of soot aggregates from the burning of typical solid and liquid fuels, Journal of Nanoparticle Research 19 (3) (2017) 96. doi:10.1007/s11051-017-3786-x.